

# King Saud University

# **Arabian Journal of Chemistry**

www.ksu.edu.sa www.sciencedirect.com



# **ORIGINAL ARTICLE**

# Preparation of purified spent coffee ground and its reinforcement in natural rubber composite



Peerayut Tapangnoi <sup>a</sup>, Pongdhorn Sae-Oui <sup>b</sup>, Weerawut Naebpetch <sup>c</sup>, Chomsri Siriwong <sup>a</sup>,\*

Received 3 January 2022; accepted 10 April 2022 Available online 18 April 2022

#### **KEYWORDS**

Spent coffee ground; Natural rubber; Eco-friendly filler; Purification; Mechanical properties; Surface modification Abstract Spent coffee ground (SCG) contains a variety of organic compounds such as fatty acids, amino acids, polyphenols, polysaccharides, etc. In this study, purification of SCG was carried out by alkalization and bleaching treatment and the purified SCG (PSCG) was characterized by various techniques, i.e., FTIR, XRD, BET, SEM and TGA. PSCG was later treated with Bistriethoxysilylpropyl tetrasulfide (TESPT). Both PSCG and TESPT-treated PSCG were then incorporated into natural rubber (NR) to investigate their reinforcement magnitude in the biocomposite. Results revealed the eradication of lignin and other non-polysaccharide components after the purification leading to the significant increases in specific surface area and cellulose content of PSCG. Although the addition of PSCG into NR showed cure time reduction in association with the increased modulus and hardness, its reinforcement was not very high due to the large particle size and the abundance of hydroxyl groups in PSCG. The TESPT treatment significantly improved the reinforcement of PSCG due to the increases in rubber-filler interaction and crosslink density. However, the reinforcement of both PSCG and TESPT-treated PSCG is still relatively low compared to the commercial nanofillers and, thus, they can be considered as a cheap and ecofriendly filler in NR.

© 2022 The Author(s). Published by Elsevier B.V. on behalf of King Saud University. This is an open access article under the CC BY-NC-ND license (http://creativecommons.org/licenses/by-nc-nd/4.0/).

E-mail address: schoms@kku.ac.th (C. Siriwong).
Peer review under responsibility of King Saud University.



Production and hosting by Elsevier

#### 1. Introduction

With the intention to alleviate environmental problems, various biofillers have been developed to replace petroleum-based fillers, *i.e.*, carbon black (CB), in the rubber reinforcement (Gardiner et al., 2001; Niranjan and Thakur, 2017). The use of bio-fillers provides many ecological benefits because they are abundant, easily available, renewable

<sup>&</sup>lt;sup>a</sup> Materials Chemistry Research Center, Department of Chemistry and Center of Excellence for Innovation in Chemistry, Faculty of Science, Khon Kaen University, Khon Kaen 40002, Thailand

<sup>&</sup>lt;sup>b</sup> National Metal and Materials Technology Center (MTEC), National Science and Technology Development Agency (NSTDA), Pathum Thani 12120, Thailand

<sup>&</sup>lt;sup>c</sup> Center of Rubber Technology for Community, Faculty of Engineering, Thaksin University, Phatthalung campus, Phatthalung 93210, Thailand

<sup>\*</sup> Corresponding author.

and, most importantly, biodegradable (Mokhothu and John, 2017; Isikgor and Becer, 2015; Gaidukova et al., 2021. Bio-fillers including their derivatives are commonly produced from many resources, for instance, sugarcane, corn, starch, rice husk, wood pulp, *etc.* (Barana et al., 2019; Bodirlau et al., 2013; Mansor and Ali, 2016; Ghani et al., 2019; Azwar and Hakkarainen, 2012; Ruangudomsakul et al., 2013; Santos et al., 2014). These materials mainly consist of cellulosic components such as cellulose, hemicellulose, and lignin.

At present, coffee is one of the most popular beverages, being largely consumed all over the world. With rapid growth of the coffee industry, the amount of spent coffee ground (SCG), a residual from the instant coffee preparation, has sharply increased which is expected to be more than 6 million tons per year (Mussatto et al., 2011a; Murthy and Naidu, 2012). Improper disposal of SCG into the environment, i.e., dumping into landfills and sewage, might cause serious pollution problems because it can leach into water sources and result in marine eutrophication which can result in excessive algae generation due to the highly nitrous compounds produced from SCG (Fernandes et al., 2017, Murthy and Naidu, 2012). In addition, the decomposition of SCG in the landfills creates methane, a greenhouse gas, and contribute to global warming (Crumbley, 2009; Cameron and O'Malley, 2016; Massaro Sousa and Ferreira, 2019). The fermentation of SCGs might also cause spontaneous combustion (Silva et al., 1998). Many attempts have therefore been made to explore the potential applications and make full use of SCG. So far, SCG has been used as a biomass fuel in boilers due to its high calorific power (Silva et al., 1998), a substrate for microorganism cultivation (Machado et al., 2012), and a raw material for ethanol production (Mussatto et al., 2012).

In addition to these applications, extensive investigation has been carried out to study the exploitation of SCG as a filler in the production of polymer composites with the intention to add value to the useless waste and decrease a negative impact on the environment (Banu et al., 2020; McNutt and He, 2019). So far, SCG has been used as a filler in various polymers such as natural rubber (NR), polyvinyl alcohol (PVA), polylactide (PLA) and polypropylene (PP) (Siriwong et al., 2018; Kyung Lee et al., 2015; Wu, 2015; García et al., 2018). However, like other bio-based fillers, the reinforcement of SCG is unsatisfactory due to its high hydrophilicity making it incompatible with most nonpolar polymers. It has been reported that SCG is generally composed of 39.1% hemicellulose, 12.4% cellulose, 23.9% lignin, 17.4% protein, 2.3% fat and traces of ashes and minerals such as potassium, magnesium, phosphorous, etc. (Ballesteros et al., 2014). The polysaccharides in SCG are formed by polymerization of a variety of sugars. In terms of polysaccharide's composition, SCG contains approximately 76% of hemicellulose (37% mannose, 32% galactose and 7% arabinose) and about 24% of cellulose (glucose) (Ballesteros et al., 2014). Similar values have also been reported by Mussatto et al. (2011b,c. Variation in these values generally arises from the differences in coffee bean type and extraction process. The poor interaction with many polymers generally results in unsatisfactory mechanical properties of the composites (Arifuzzaman Khan et al., 2013; Saba et al., 2016). This limits the large-scale use of SCG as a bio-filler in polymer composites (Vaisanen et al., 2017). Surface modification of SCG is therefore required to improve interfacial interaction. Previous works have revealed the enhanced mechanical properties of the SCG composites when SCG is surface-treated by maleic anhydride, etc. (Wu, 2015; Baek et al., 2013; Tan et al., 2017).

As SCG is a mixture of a variety of organic compounds such as cellulose, hemicellulose, lignin, protein and fatty acids, the surface modification of SCG by coupling agent or maleic anhydride is therefore complicated and ineffective. It is of great interest to extract each individual component of SCG and explore it potential use as a bio-filler for polymer composites (Pujol et al., 2013; Ballesteros et al., 2014). Recently, attempts to purify SCG by alkalization and bleaching treatment have been made by Essabir, et al. (2018). Reinforcement of the obtained SCG in polypropylene was then investigated. They revealed the improvement of interfacial interaction after bleaching treatment and the finding is even more pronounced in the presence of a coupling agent.

Although the reinforcement of SCG in various polymers has been extensive investigated, the effect of purified SCG (PSCG) on properties of NR has not been reported. This work therefore aimed to purify SCG via alkalization and bleaching treatment to eliminate lignin and other non-polysaccharide components using the procedures described by Essabir, et al. (2018). The prepared PSCG was later characterized by various techniques including SEM, FTIR, XRD, BET, etc. Both PSCG and surface-treated PSCG were then incorporated into NR at different loadings to investigate the effects of filler loading and surface treatment on mechanical properties of the PSCG-filled NR composites.

#### 2. Experimental

#### 2.1. Materials

Natural rubber (STR, 5L) was purchased from Srijaroen Co., Ltd., Bangkok, Thailand. The spent coffee ground (SCG), obtained from local coffee shops in Khon Kaen, Thailand, was milled and sieved through 80 mesh. Sodium hydroxide (NaOH), acetic acid (CH<sub>3</sub>COOH), nitric acid (HNO<sub>3</sub>), acetone, ethanol (C<sub>2</sub>H<sub>5</sub>OH) and sodium chlorite (NaClO<sub>2</sub>) were obtained from QRëC, New Zealand. *Bis*-(triethoxysilylpropyl) tetrasulfide (TESPT) was manufactured by Evonik Co., Ltd., Essen, Germany. All other chemicals for NR compounding, such as sulfur, zinc oxide (ZnO), stearic acid, and N-cyclohexyl-2-benzothiazole sulfenamide (CBS) were supplied by Reliance Technochem Co., Ltd., Nakhonpathom, Thailand. All chemicals were used as received without further purification.

## 2.2. Purification of SCG

Alkalization was carried out by adding 30 g of SCG into 300 mL of 5% sodium hydroxide solution (NaOH) under a continuous stirring at 70 °C for 2 h. Thereafter, the SCG was washed thoroughly with distilled water to completely remove the remaining hydroxide. The alkali-treated SCG was later dried in an oven at 80 °C for 24 h. A bleaching treatment was then performed to remove lignin in SCG by mixing it with a bleaching agent, a mixed solution of acetate buffer and sodium chlorite solution (1:1 v/v), at 80 °C for 2 h. This treatment was repeated 3 times to ensure a complete removal of lignin. The suspension was subsequently washed with distilled water many times by using centrifugation technique until pH of the washed water was neutral. The suspension was then homogenized by a homogenizer (HG-15A, Daihan Scientific, Korea) 500 rpm for 1 h and, finally, freeze dried to obtain PSCG. The % yield of the purification process was calculated using Eq. (1):

$$Yield(\%) = \frac{W_f}{W_i} \times 100 \tag{1}$$

where  $W_i$  is the weight of dried SCG and  $W_f$  is the weight of dried PSCG.

## 2.3. Preparation of TESPT-treated PSCG

The PSCG sample was surface-treated by TESPT using the procedures described in the literature (Xiao et al., 2020). Initially, PSCG was mixed with TESPT in a container with the mass ratio of PSCG to TESPT of 40:3.2. To obtain a uniform

mixture, mixing was carried out in a high-speed multifunctional grinder for 30 min. The mixture was later heated in an oven at 120 °C for 1 h to complete the reaction. In the end, the TESPT-treated PSCG was transferred into a beaker, mixed with anhydrous ethanol, and stirred to remove the unreacted TESPT. The TESPT-treated PSCG was finally filtered, dried at 60 °C for 24 h in an oven until a constant weight was achieved prior to being used.

#### 2.4. Filler characterization

Determination of cellulose content in PSCG was carried out according to the method described by Brendel et al. (2000). Initially, 10 g of PSCG were mixed with 2.0 mL of acetic acid (80% v/v) and 0.2 mL of concentrated nitric acid (69% v/v) in a screw-capped tube, and autoclaved at 120 °C for 20 min. After cooling, the cleaning process was carried out by adding 2.5 mL of a cleaning liquid into the suspension, centrifuging the mixture and then discarding the supernatant. The cleaning process was repeated six times by using 99% v/v of ethanol as a cleaning liquid during the first two times and followed by deionized water (two times) and, finally, acetone during the last two times. After cleaning, the solid residue (cellulose) was dried in an oven at 80 °C for 24 h prior to weighing. The cellulose content was calculated as the weight percentage of solid residue to initial sample.

Surface functional groups of SCG, PSCG and TESPT-treated PSCG were determined by Fourier transform infrared (FTIR) spectrophotometer (Bruker Tensor 27, Ettlingen, Germany), equipped with an attenuated total reflectance (ATR). Each spectrum was obtained from an accumulation of 16 scans with a resolution of 4 cm<sup>-1</sup>. Crystal structure was studied by X-ray diffraction (XRD, Malvern Panalytical Co., Ltd., Royston, UK) using Cu-K $\alpha$  radiation ( $\lambda$  = 0.15406 nm) with a diffraction angle range of 5°–50°. The crystallinity index (*CrI*) was determined by Segal method as illustrated in Eq. (2) (Segal et al., 1959).

$$CrI(\%) = \frac{I_{002} - I_{am}}{I_{002}} \times 100$$
 (2)

where  $I_{002}$  and  $I_{am}$  are the peak intensity of (002) crystallographic plane ( $2\theta = 21.6^{\circ}$ ) and the peak intensity of the amorphous domain ( $2\theta = 18^{\circ}$ ), respectively.

Thermal behaviors of all samples were characterized by a thermogravimetric analyzer (TGA, STA7200 Hitachi, Tokyo, Japan) under a nitrogen atmosphere from 30 to 700 °C at a heating rate of 10 °C/min. Morphology of the samples was studied by a desktop scanning electron microscope (mini-SEM, SEC Co., Ltd. KyungGi-Do, South Korea). The samples were sputter coated with gold to avoid electron bombardment prior to the examination. Specific surface area was determined by the Brunauer-Emmett-Teller (BET) method using an Autosorb-1 (Quantachrom; Florida, USA). Density of SCG were measured by Ultrapycnometer-1000 (Florida, USA). Determination of particle size confirmation was performed by using the Mastersizer-S (Malvern; Worcestershire, UK). Measurement of pH was carried out by stirring 5 g of the filler in 50 mL of hot distilled water for 30 min and pH of the suspension was measured by a pH meter (Schott; Trutnov, Czech Republic). The amounts of carbon (C), hydrogen (H), and nitrogen (N) in the SCG and PSCG samples were measured by CHNS/O elemental analyzer (Perkin Elmer (Series II), MA, USA).

#### 2.5. Preparation and testing of NR composites

The compound formulations are tabulated in Table 1. Mixing was carried out for 12 min on two-roll mill (Chaicharoen Karnchang Ltd., Bangkok, Thailand) at a set temperature of 35 °C. Initially, rubber was masticated on the two-roll mill for 2 min before adding filler together with activators and, finally, curatives. The rubber compounds were kept overnight prior to being tested.

Measurement of bound rubber content (BRC), defined as the amount of rubber tightly attached on the filler's surface and cannot be extracted by a good solvent for rubber, was conducted by soaking approximately 1 g of the uncured rubber specimen in 100 mL of toluene at standard laboratory temperature (25 °C) for 7 days. The bound rubber-filler gel was then filtered by Buchner vacuum filter, dried overnight in an aircirculating oven at 80 °C and weighed. The BRC was calculated by Eq. (3);

$$BRC (\%) = \frac{\left[W_{fg} - W[m_f/(m_f + m_r)]\right]}{W[m_f/(m_f + m_r)]} \times 100$$
 (3)

where  $W_{fg}$  is the weight of rubber-filler gel, W is the specimen weight before soaking while  $m_f$  and  $m_r$  are the weights of filler and rubber in the formulation, respectively.

Cure characteristics of the rubber compounds, i.e., scorch time (t<sub>s2</sub>) and optimum cure time (t<sub>c</sub>90), minimum torque (M<sub>L</sub>), and maximum torque (M<sub>H</sub>), were determined at 150 °C by a moving die rheometer (MDR-01, CG Engineering Co., Ltd., Pathum Thani, Thailand) according to ISO 6502-3. The torque difference  $(M_H - M_I)$  is used to represent indirectly the crosslink density of the vulcanizates. Vulcanized rubber sheets were subsequently prepared by compression molding technique using a hydraulic press machine (3114 Engineering Co., Ltd., Bangkok, Thailand) at 150 °C for the corresponding optimum cure time (t<sub>c</sub>90) previously determined from the MDR. The vulcanized rubbers were left at standard laboratory temperature at least 24 h prior to testing. Hardness of the vulcanizates was measured by a durometer (H17A, Wallace instrument, UK) with Shore A scale as per ISO 48-4. Tensile test was performed using a universal testing machine (UTM 5567A, Instron instruments Inc., MA, USA) according to ISO 37 (die type I). To evaluate the approximate values of

Table 1   Rubber formulations.					
Ingredients	Content (phr <sup>a</sup> )	Function			
NR	100	Rubber			
PSCG or TESPT-treated	Varied (0, 5, 10, 15,	Filler			
PSCG	20)				
ZnO	5	Cure activator			
Stearic acid	2	Cure activator			
CBS	1	Cure			
		accelerator			
Sulfur	1.75	Vulcanizing			
		agent			
a phr = parts per hundred rubber.					

crosslink density, three specimens with the approximate dimensions of 10x10x2 mm<sup>3</sup> were prepared, weighed, and immersed in toluene at standard laboratory temperature for 7 days. Subsequently, each specimen was wiped with towel paper and immediately weighed. The specimens were later dried in an oven at 80 °C until a constant weight was gained. The apparent crosslink density was calculated by Flory-Rehner equation as follows.

$$v = \frac{-[\ln(1 - \phi_p) + \phi_p + \chi \phi_p^2]}{[V_1(\phi_p^{1/3} - \phi_p)/2]}$$
(4)

Herein, v is the crosslink density (mol/m<sup>3</sup>),  $V_1$  is the molar volume of toluene (106.3 cm<sup>3</sup>/mol),  $\chi$  is Flory-Huggins interaction parameter between toluene and rubber (0.378) and  $\phi_p$  is the volume fraction of swollen rubber. By assuming that only the rubber chains can swell in toluene,  $\phi_p$  can be calculated by Eq. (5);

$$\phi_p = \frac{(m_2 \times m_r)/\rho_r}{(m_2 \times m_r)/\rho_r + (m_2 \times m_f)/\rho_f + (m_1 - m_2)/\rho_s}$$
 (5)

where  $m_1$  and  $m_2$  are the specimen's weights in the swollen and un-swollen states, and  $\rho_r$ ,  $\rho_s$  and  $\rho_f$  are densities of the rubber, solvent and filler, respectively. The parameters of  $m_r$  and  $m_f$  denote the mass ratio of rubber and filler in the un-swollen compounds.

The water absorption (WA) of the filled NR composites was measured using the procedures described by Ahmed, et al. (2012). The specimens were first dried at 60 °C under vacuum for 24 h, weighed and then immersed in deionized water at room temperature for various time intervals (0.25, 0.5, 1, 3, 5, 7 and 14 days). The specimens were subsequently removed from the deionized water and wiped softly with filter paper to eliminate any water droplet on the specimen's surface prior to being weighed. The value of WA was calculated using Eq. (6).

$$WA(\%) = \frac{W_1 - W_0}{W_0} \times 100 \tag{6}$$

where  $W_0$  and  $W_1$  are the specimen's weights before and after water immersion.

#### 3. Results and discussion

### 3.1. Filler preparation and characterization

Fig. 1 shows photographs, SEM images and particle size distribution of all filler used. Before purification, SCG is a dark brown powder and, when magnified under SEM, its particles are relatively large and irregular. The results are in good agreement with those previously reported in the literature (Siriwong et al., 2017; Conde and Mussatto, 2016). After purification, 29% yield of PSCG is obtained. The color of SCG changes from dark brown into light yellow, probably due to the consequence from delignification. It is also obvious from the SEM images that purification causes an increase in surface roughness because of the elimination of lignin and other nonpolysaccharides from the SCG particles. This leads to a significant increase in BET specific surface area (from 3.7 to 6.1 m²/g) in association with a small decrease in particle size (from 59.0 to 52.6 μm) as shown in Table 2. However, the results

reveal that the purification does not significantly affect pH and density of SCG. In addition, the results from CHNS/O analysis reveal that SCG contains approximately 51.1% C, 8.0% H and 2.1 % N. Similar values have previously been reported (Colantoni et al., 2021). After the purification, the amounts of C and H increase slightly to 54.0% and 9.6%, respectively. The amount of N, on the other hand, considerably reduces from 2.1% to 0.2% indicating the substantial reduction (greater than90%) of nitrogen-containing compounds, such as protein and caffeine, in SCG after the purification. The results, however, imply that the purification method used herein cannot completely remove all these nitrogen-containing compounds in the SCG sample.

The FTIR spectra of SCG and PSCG are shown in Fig. 2a. For SCG, the broad peak at 3363 cm<sup>-1</sup> is attributed to O-H stretching of polysaccharide, fatty acids and polyphenols (Siriwong et al., 2017; Lu et al., 2013; Lu et al., 2014). The strong peaks at 2920 and 2851 cm<sup>-1</sup> are assigned to C-H stretching vibration while the peak at 1487 cm<sup>-1</sup> is assigned to C-H bending vibration. The small peak at 3050 cm<sup>-1</sup> is also observed, attributed to the C-H stretching vibration of aromatic hydrocarbon in lignin. The peaks at 1710 and  $1614 \text{ cm}^{-1}$  are respectively referred to C = O and C = C stretching vibrations of caffeine, hemicellulose, and chlorogenic acid. The peak at 1583 cm<sup>-1</sup> is attributed to C-N stretching vibration of protein or amino. The peak at 1398 cm<sup>-1</sup> belongs to COO symmetric stretching vibration. The peak at 1252 cm<sup>-1</sup> is assigned to C-O vibration from lignin. The peaks at 1015 cm<sup>-1</sup> and 736 are assigned to C-O-C and C-O groups from cellulosic components and lignin (Siriwong et al., 2017). For PSCG, the disappearance of the peak at 3050 cm<sup>-1</sup> assigned to C-H vibration of aromatic hydrocarbon, and the significant reduction of the peak at 1614 cm<sup>-1</sup> assigned to C = C vibration of lignin and other aromatic compounds indicate the effective removal of lignin and other nonpolysaccharide components after the purification. The noticeable reduction of the C-N stretching vibration peak at 1583 cm<sup>-1</sup> is also observed confirming the considerable reduction of protein and caffeine after the purification.

As previously mentioned, SCG contains many components such as crystallizable cellulose and non-crystallizable hemicellulose and lignin. SCG is therefore classified as a semicrystalline material, consisting of both crystalline and amorphous regions. XRD patterns of SCG and PSCG are given in Fig. 2b. Obviously the XRD spectrum of SCG shows peaks at  $2\theta = 16.1^{\circ}$  and  $21.6^{\circ}$  which correspond to the (101) and (002) crystallographic planes of cellulose, respectively. After the purification, the magnitude of these crystalline peaks increases significantly due to the removal of amorphous lignin and, perhaps, a portion of hemicellulose (Kargarzadeh et al., 2012). It is noted that the purification process does not affect the crystal structure of cellulose in SCG. From the XRD patterns, crystallinity index (CrI) can be calculated from Eq. (2). The results reveal that the CrI values are approximately 2.6% and 17.8% for SCG and PSCG, respectively. The increase in CrI is easily understandable because the purification process considerably removes the amorphous portion of SCG leading to the significant increase in cellulose fraction and, thus, the higher CrI value. The results agree well with the literature (El Miri et al., 2015; Kargarzadeh et al., 2012).

TGA and DTG curves of SCG and PSCG are illustrated in Fig. 3. The results show that the decomposition of SCG can be

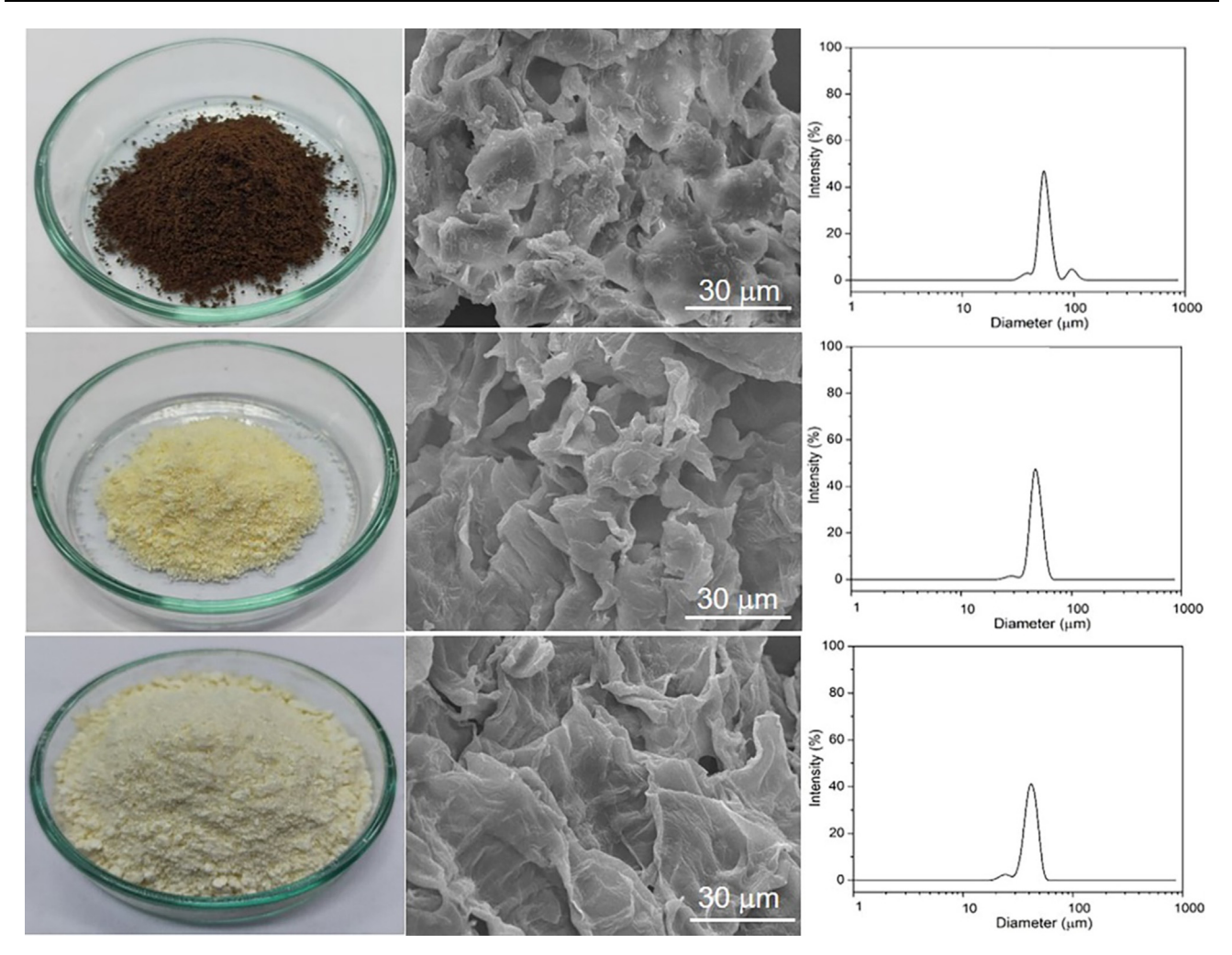


Fig. 1 Photographs, SEM images and particle size distribution of the samples; SCG (top), PSCG (middle) and TESPT-treated PSCG (bottom).

Table 2         Basic properties of the samples.			
Property	SCG	PSCG	TESPT-treated PSCG
BET specific surface area (m <sup>2</sup> /g)	$3.7 \pm 0.3$	$6.1 \pm 0.1$	$8.5 \pm 0.3$
Average particle size (µm)	$59.0 \pm 2.7$	$52.6 \pm 3.5$	$50.3 \pm 1.8$
pH	$6.9 \pm 0.1$	$6.7 \pm 0.2$	$6.8 \pm 0.1$
Density (g/cm <sup>3</sup> )	$0.92 \pm 0.01$	$0.92 \pm 0.01$	$0.92 \pm 0.02$

divided into many stages (Essabir et al., 2013a,b; Moustafa et al., 2017). The initial mass loss occurring at 50–150 °C (approximately 6.6%) is attributed to the evaporation of moisture adsorbed on the SCG surface (Ballesteros et al., 2015; Essabir et al., 2017). The second mass loss found at the temperature range between 150 and 250 °C (approximately 8.5%) is related to the thermal depolymerization of hemicellulose (García-García et al., 2015). The third mass loss is found at the temperature range of 250–400 °C with a mass loss of approximately 45.5%, corresponding to the decomposition of the major constituents of SCG, *i.e.*, hemicellulose and cellulose (Siriwong et al., 2017; Essabir et al., 2016). The final mass loss found at the temperature above 400 °C is due to the decomposition of lignin and other organic compounds with stronger chemical

bonds (Lu et al., 2014; Cardenas-Aguiar et al., 2017). As lignin is full of various branched aromatic rings making it difficult to decompose, the decomposition of lignin therefore takes place very slowly over a wide temperature range (Yang et al., 2007). At the end of the test, approximately 27.4% of residue is observed for SCG sample. This residue is a mixture of char and inorganic alkalis (Boopasiri et al., 2021; Campos-Vega et al., 2015; Sung et al., 2017). The presence of char in SCG sample after the pyrolysis is not uncommon because SCG contains significant amounts of aromatic hydrocarbons (lignin) and nitrogen-containing compounds such as proteins, caffeine and free amines, which can facilitate the char formation during the pyrolysis (Sung et al., 2017; Das et al., 2016). After the purification, a similar decomposition behavior is observed.

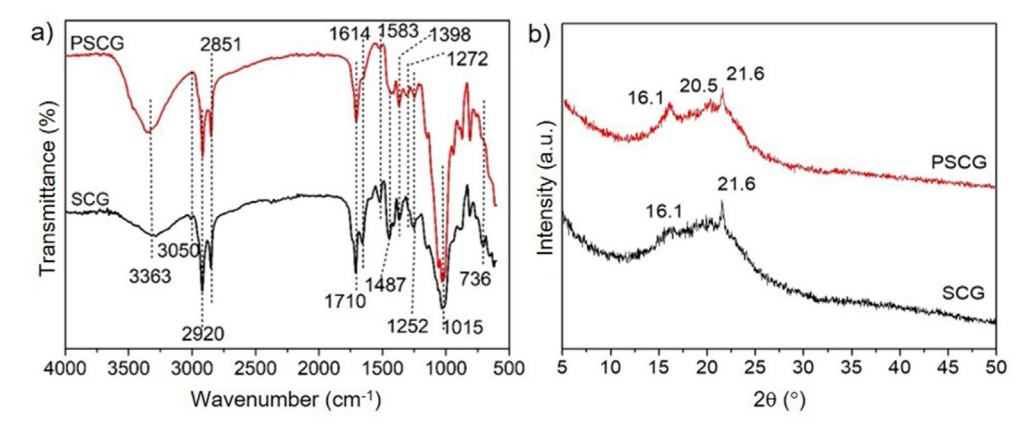


Fig. 2 FTIR spectra (a) and XRD patterns (b) of the samples.

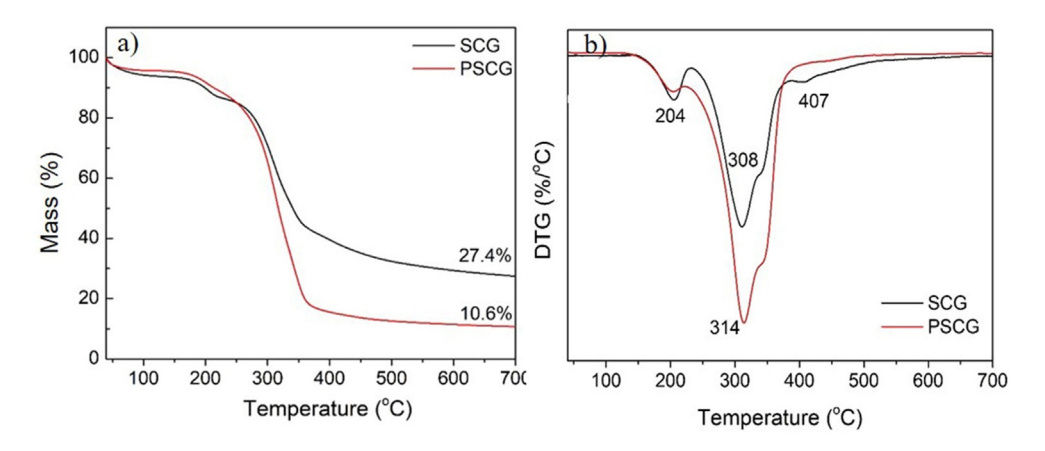


Fig. 3 Thermograms of SCG and PSCG; TGA curves (a) and DTG curves (b).

However, due to the absence of lignin and other nonpolysaccharide components in PSCG, the residue content is significantly reduced (from 27.4 to 10.6%) in conjunction with the increase in the proportion of mass loss at 150–400 °C, representing the amount of cellulose and hemicellulose in the PSCG sample. The DTG curves in Fig. 2b display the maximum decomposition temperatures (T<sub>d</sub>) of the samples. Clearly, T<sub>d</sub> peak found at 204 °C is related the depolymerization of hemicellulose while the one found at 308-314 °C represents the decomposition of cellulose and hemicellulose. The small T<sub>d</sub> peak observed in the SCG sample at 407 °C is probably due to the decomposition of lignin which disappears after the purification confirming the absence of lignin in PSCG. Calculation of the cellulose content in the samples reveals the significant increase in cellulose content from approximately 12% in SCG to approximately 30% in PSCG. Such increase is attributed to the removal of lignin and other nonpolysaccharide components from SCG after the purification.

## 3.2. Surface modification of PSCG

FTIR spectra of PSCG and TESPT-treated PSCG are displayed in Fig. 4a. Peak identification of PSCG is previously given. Apparently, the FTIR spectra of both samples are

almost identical. Theoretically, a new absorption peak of Si-O-C should appear at 1015 cm<sup>-1</sup> after the modification. Unfortunately, such peak overlaps with the broad vibration peaks of C-O-C and C-O of cellulose or hemicellulose. Lu et. al. previously reported a similar observation in which there was no significant change in FTIR spectrum of cellulose after the TESPT treatment (Lu et al., 2014). However, it can be observed that, after the TESPT treatment, there is an increase in the intensity ratio of C-H stretching peak (at 2920 cm<sup>-1</sup>) to O-H stretching peak (at 3404 cm<sup>-1</sup>), i.e., increasing from 1.35 to 1.46, indicating the increased fraction of methylene groups after the treatment which comes from TESPT. Fig. 4b displays XRD patterns of PSCG and TESPT-treated PSCG. Obviously, both samples show the same XRD pattern, possessing peaks at 16.1°, 20.5°, and 21.6°, assigned respectively to the (110), (021) and (002) crystallographic planes of cellulose (Frost and Foster, 2020). The degree of crystallinity, however, reduces slightly from 17.8% to 15.5% after the TESPT treatment. It has previously been reported that the reaction between any reagent and cellulose generally occurs either in the amorphous regions or at the edges of the crystalline regions of cellulose, *i.e.*, the reagent initially reacts with the chain ends on the surface of crystallites, giving rise to the opening of some of the hydrogen-bonded cellulose chains, resulting in a conver-

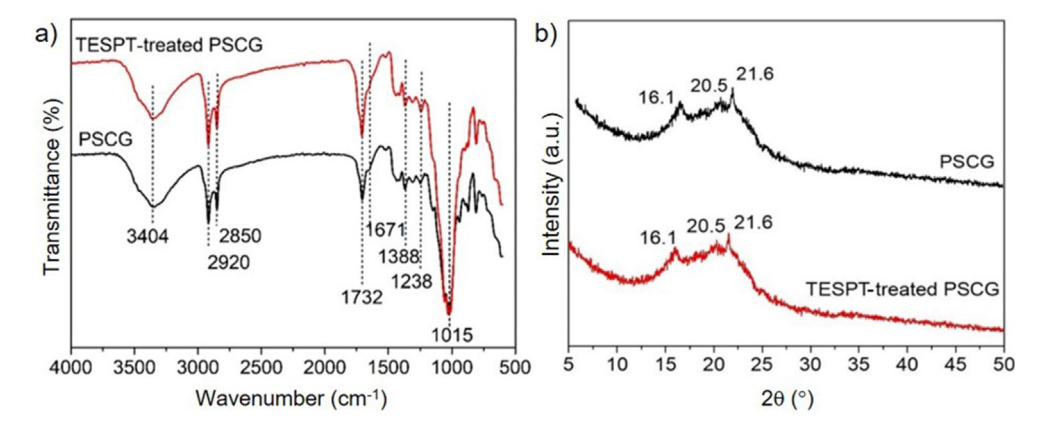


Fig. 4 FTIR spectra (a) and XRD patterns (b) of PSCG and TESPT-treated PSCG.

sion of some crystalline cellulose to amorphous cellulose (Cao et al., 2018; Zhou et al., 2014).

Thermal behaviors of PSCG and TESPT-treated PSCG, analyzed by TGA, are compared as shown in Fig. 5. Apparently, the TESPT-treated PSCG decomposes in a similar manner to PSCG. However, the residue content at 700 °C of TESPT-treated PSCG is slightly higher than that of PSCG. The results are not beyond expectation because pyrolysis of TESPT generally gives very high content of silica (SiO<sub>2</sub>), approximately 4.9%, which is the main inorganic residue (ash) for TESPT. The attachment of TESPT on PSCG therefore slightly increases the ash content after the pyrolysis.

## 3.3. Properties of the NR composites

The relationship between bound rubber content (BRC) and filler loading is illustrated in Fig. 6. As can be expected, BRC increases with increasing filler loadings, regardless of the filler type, which can be explained by the increased contact surface area of filler at higher filler loadings. At any given filler loading, PSCG gives lower BRC due to the existence of polar hydroxyl groups on its surface leading to the great discrepancy in polarity between PSCG and NR. When PSCG is treated with TESPT, a higher BRC is observed. The greater rubber–filler interaction obtained by TESPT treatment is thought to arise from the reduced surface polarity of PSCG taking place from the chemical reaction between alkoxy groups of TESPT

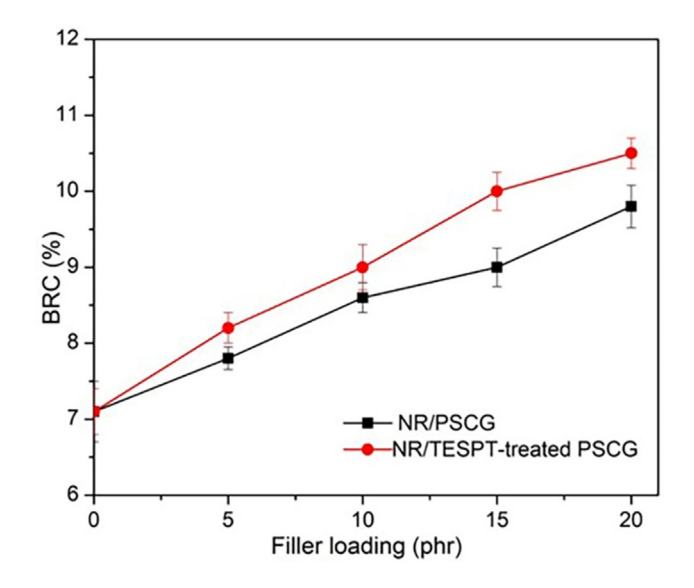


Fig. 6 Bound rubber content against filler loading of the sample.

and hydroxyl groups on the PSCG surface as revealed in Fig. 7. In addition, a slight increase in specific surface area after the TESPT treatment (Table 2), due to the grinding action during the treatment, might be another reason for the increased rubber-filler interaction.

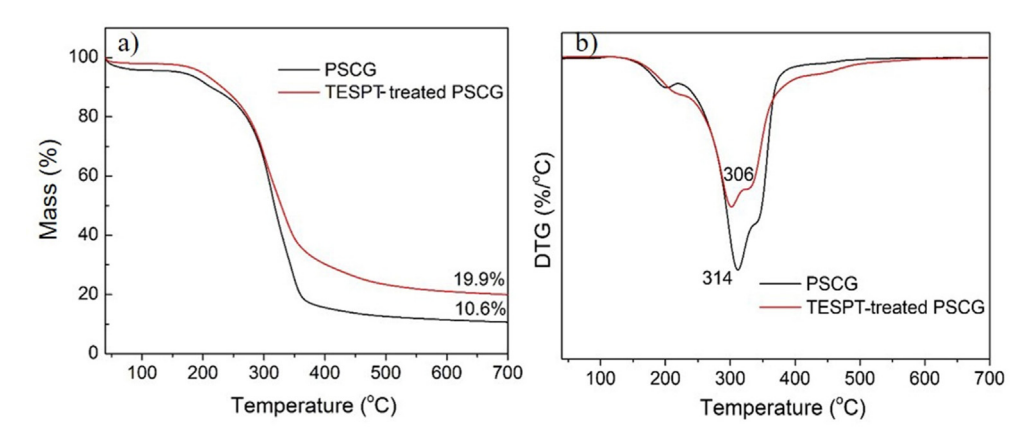


Fig. 5 TGA (a) and DTG (b) of PSCG, and TESPT-treated PSCG.

Purified SCG cellulose (PSCG)

+ 
$$C_2H_5O$$
 $C_2H_5O$ 
 $C_2H_5O$ 

Fig. 7 Proposed mechanism of interaction between PSCG and TESPT.

Cure characteristics of the NR compounds filled with PSCG and TESPT-treated PSCG are displayed in Fig. 8. The cure curves of the NR/PSCG and NR/TESPT-treated PSCG composites are given in Fig. 8a and 8b. Both scorch time  $(t_{s2})$  and optimum cure time  $(t_{c}90)$ , extracted from the cure curves (see Fig. 8c), decrease continuously with increasing filler loading, regardless of the filler type. Although the hydroxyl groups on the filler's surface are known to adsorb zinc complex and basic accelerators which generally result in cure retardation, contrary results are found herein. Explanation is given by the dominant effect taking place from the release of moisture adsorbed on the filler's surface which could facilitate the dissociation of accelerator, particularly the sulfenamide type, leading to the shorter scorch and cure times (Butler and Freakley, 1992). Similar observation has also been reported (Ahmed et al., 2013; Mostoni et al., 2019). Compared with PSCG at the same filler loading, TESPT-treated PSCG gives slightly shorter scorch time and optimum cure time. This is not beyond expectation because TESPT contains elemental sulfurs which could be released and take part in vulcanization reaction at high curing temperature. The cure acceleration in the presence of silane coupling agent has also been previously reported Dannenberg, 1985; Wagner, 1981.

The torque difference obtained from the rheometer, an indirect indicator of crosslink density, is represented in Fig. 8d. Obviously, the torque difference tends to increase with increasing filler loading. This phenomenon is thought to arise from the cure activation of the nitrogen-containing compounds in

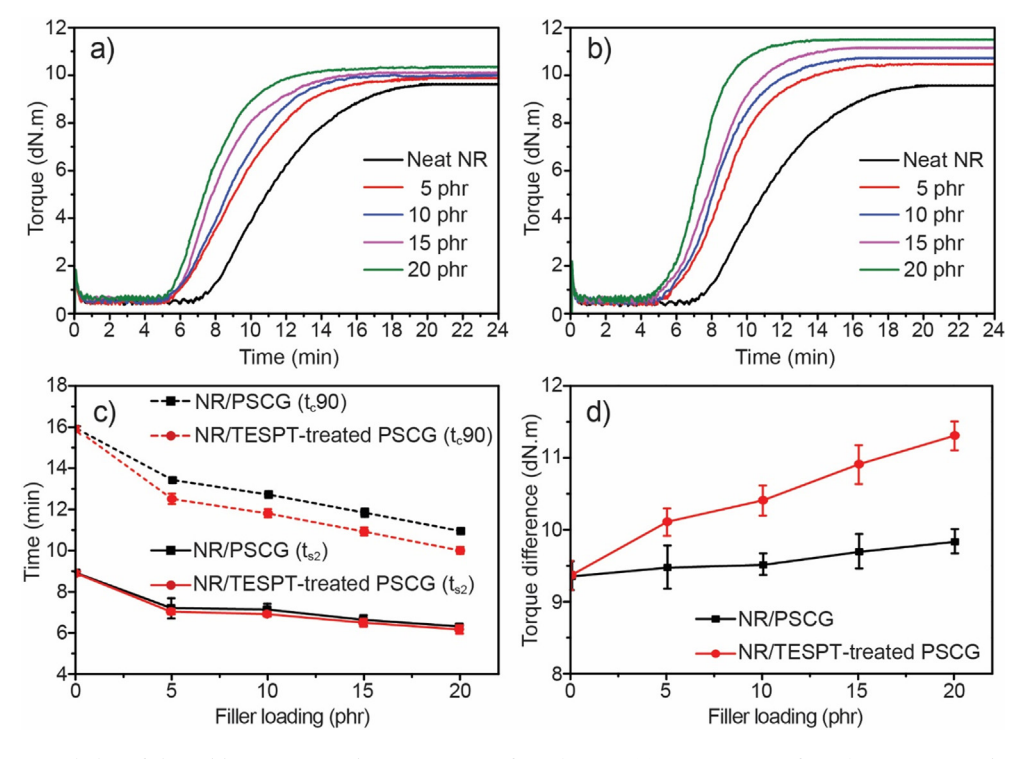


Fig. 8 Cure characteristics of the rubber compounds: cure curves of NR/PSCG (a), cure curves of NR/TESPT treated-PSCG (b), scorch time and optimum cure time against filler loading (c), and torque difference against filler loading (d).

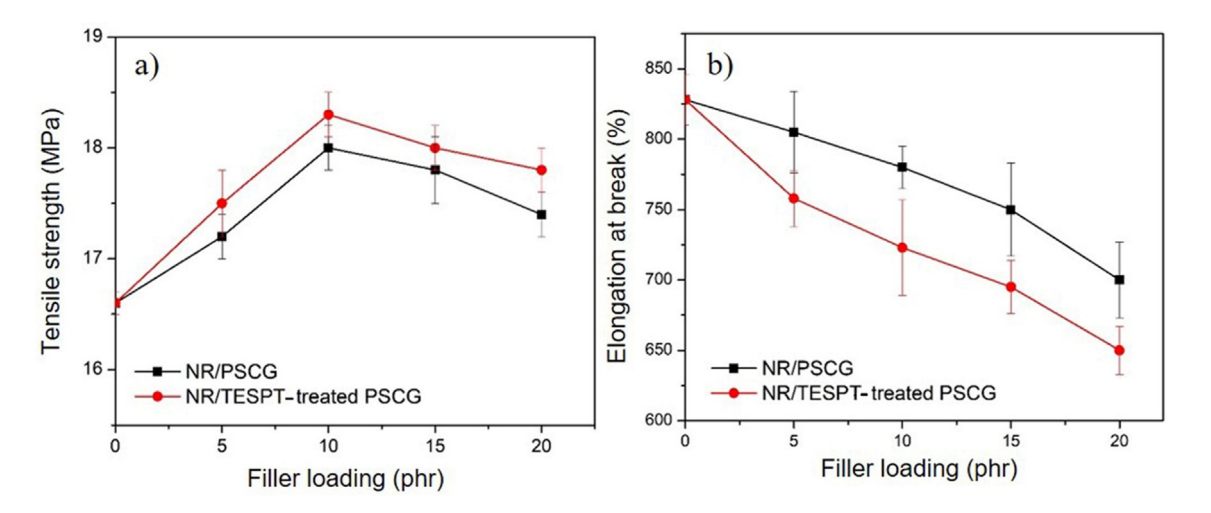
Table 3 Effect of filler type and filler loading on crosslink density, hardness and modulus of the NR composites.						
Sample	Loading (phr)	Crosslink density (x10 <sup>-4</sup> mol/cm <sup>3</sup> )	Hardness (Sh A)	M <sub>100</sub> (MPa)		
Neat NR	0	$3.50 \pm 0.02$	$29.8 \pm 0.6$	$0.57 \pm 0.03$		
NR/PSCG	5	$3.58 \pm 0.06$	$31.3 \pm 0.3$	$0.65 \pm 0.03$		
	10	$3.61 \pm 0.03$	$32.3 \pm 0.6$	$0.72 \pm 0.02$		
	15	$3.70 \pm 0.03$	$33.0 \pm 0.4$	$0.79 \pm 0.04$		
	20	$3.73 \pm 0.02$	$33.6 \pm 0.3$	$0.82 \pm 0.03$		
NR/TESTP-treated PSCG	5	$3.66 \pm 0.02$	$31.6 \pm 0.1$	$0.72 \pm 0.03$		
	10	$3.72 \pm 0.03$	$32.8 \pm 0.3$	$0.80 \pm 0.03$		
	15	$3.85 \pm 0.04$	$33.6 \pm 0.3$	$0.84 \pm 0.03$		
	20	$3.96 \pm 0.02$	$34.2 \pm 0.2$	$0.92 \pm 0.02$		

PSCG. At a given filler loading, TESPT-treated PSCG provides a higher magnitude of torque difference, possibly due to the contribution of additional sulfurs released from TESPT as previously mentioned.

Results of crosslink density, hardness and modulus at 100% strain (M<sub>100</sub>) of the NR composites are displayed in Table 3. Results show a slight increase in crosslink density with increasing filler loading. At the same filler loading, TESPTtreated PSCG exhibits slightly higher crosslink density than PSCG which could be attributed to the sulfur donor effect of TESPT during the curing process. The results agree well with the torque difference results as mentioned earlier. Similar finding has previously been reported (Sae-Oui et al., 2005; Siriwong et al., 2014).

Owing to the combination of dilution effect and increased crosslink density, both hardness and modulus increase with increasing filler loading. Indeed, the effects of many parameters on hardness and modulus generally follow the same trend because hardness and modulus are closely related, i.e., hardness is essentially a measure of modulus at low strains (Brown and Soulagnet, 2001). At any given filler loading, TESPT-treated PSCG shows slightly higher hardness and modulus than PSCG which could be attributed to the combination of the greater magnitude of rubber-filler interaction as evidenced from the BRC results and the higher crosslink density (Sinclair et al., 2019). It can be observed that approximately 5 phr of PSCG is required for every 1 unit (1 Shore A) increase in hardness of the rubber composites. Compared with the ability to increase hardness of the unpurified SCG (10 phr per 1 unit increase in hardness) reported in our previous work (Siriwong et al., 2017), PSCG exhibits a significantly greater reinforcement. However, its reinforcement is still relatively low compared to various grades of carbon black because it has previously been reported that, to increase 1 unit of hardness, natural rubber requires only 1.9, 2.5 and 4.2 phr of N330, N660 and N990, respectively Jacques, 1971.

The effect of filler loading on tensile strength and elongation at break of the NR composites is displayed in Fig. 9. Tensile strength initially increases with increasing filler loading up to 10 phr and, then, slowly declines afterwards. The initial improvement (below 10 phr) might be brought about by the increased crosslink density whereas the impairment at higher filler loadings might result from the defects of large filler particles embedded in the rubber matrix causing higher stress concentration during the tensile test. As can be expected, TESPTtreated PSCG exhibits higher tensile strength than PSCG when compared at the same filler loading. This can be explained by the higher crosslink density and the increased rubber-filler interaction in the presence of TESPT. The improved rubberfiller interaction in the NR composite filled with TESPTtreated PSCG is also supported by the SEM micrographs (Fig. 10) taken on the tensile fracture surfaces of the samples filled with 5 and 10 phr of fillers. Clearly, the SEM micrographs show the filler particles embedded in the NR matrix. A gap at rubber-filler interface can be used as an indication of poor rubber-filler interaction. Without TESPT treatment



Tensile properties of the NR composites; tensile strength (a) and elongation at break (b).

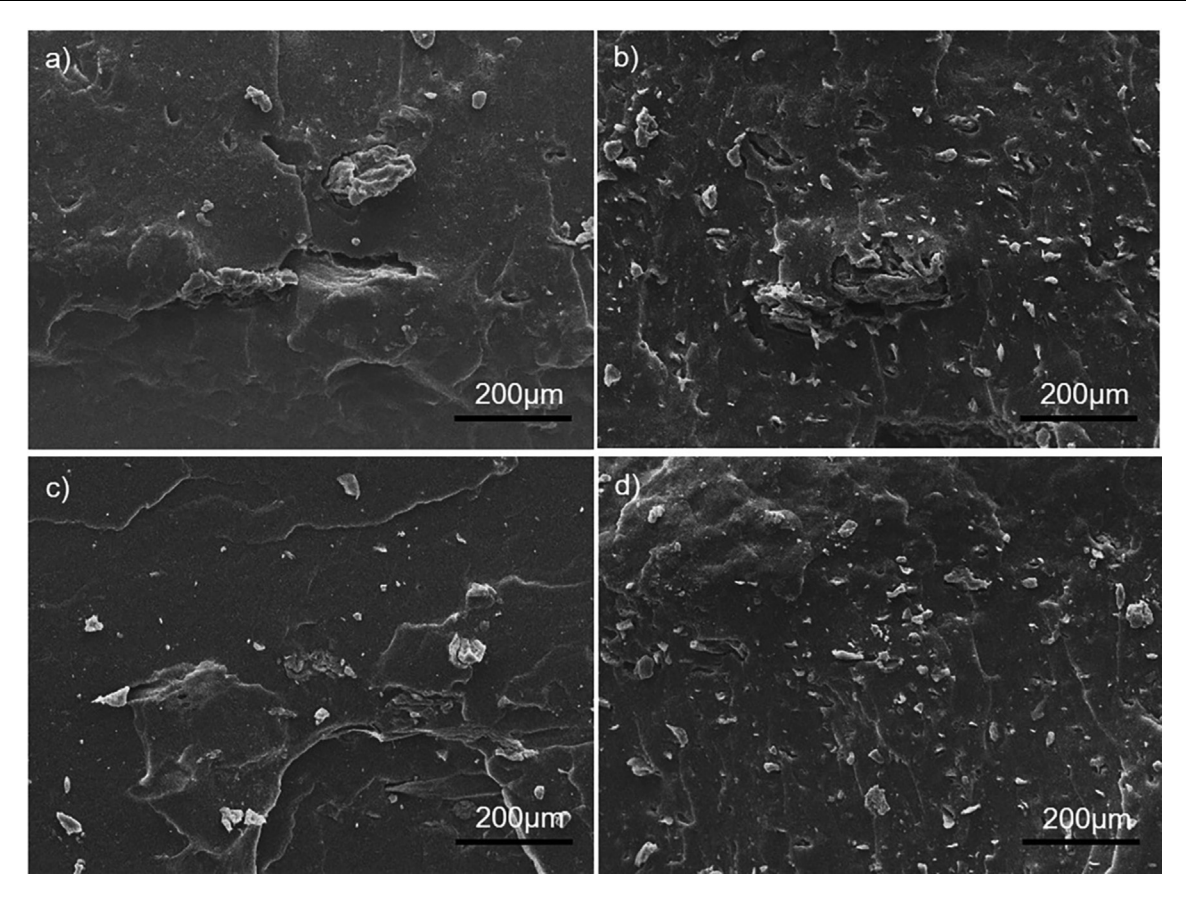


Fig. 10 SEM images of the NR composites; PSCG at 5 phr (a), PSCG at 10 phr (b), TESPT-treated PSCG at 5 phr (c) and TESPT-treated PSCG at 10 phr(d).

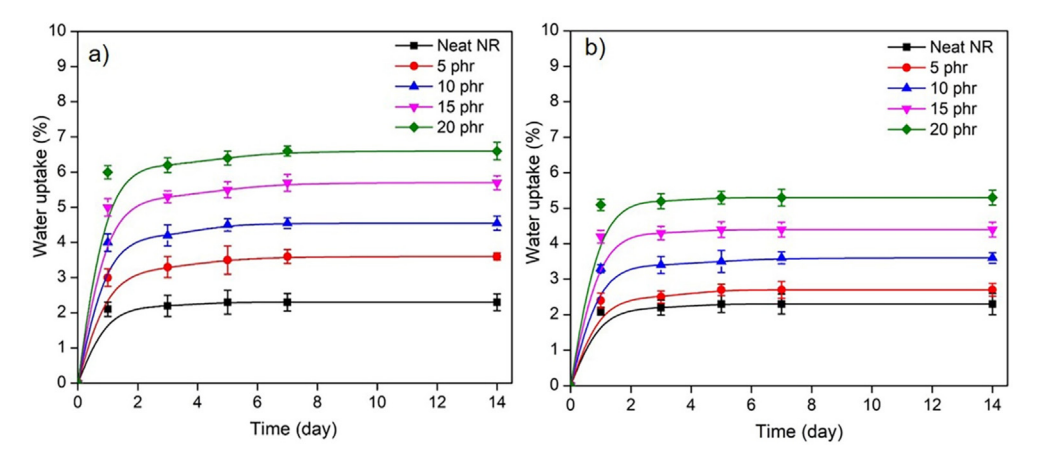


Fig. 11 Water absorption as a function of time of: NR/PSCG (a) and NR/TESPT-treated PSCG(b).

(Fig. 10a and 10b), voids around the PSCG particles are clearly visualized. Nevertheless, after the TESPT treatment (Fig. 10c and 10d), interfacial voids are less pronounced indicating the improved wettability of filler by matrix and, thus, the greater magnitude of interfacial interaction. The enhanced interfacial adhesion between filler and polymer matrix via silane surface treatment has previously been reported (Siriwong et al., 2014; Hashim et al., 1998).

The results in Fig. 9b also show the gradual reduction of elongation at break with increasing filler loading. The dilution effect and the increased crosslink density can be used to explain this finding. Clearly, TESPT-treated PSCG exhibits lower elongation at break than PSCG, at the same filler loading, possibly due to the higher crosslink density resulting from the sulfur-donor effect of TESPT as previously mentioned.

Due to the abundance of hydroxyl groups in hemicellulose and cellulose, PSCG is hydrophilic and can adsorb significant amount of water via hydrogen bonding. It is therefore of great interest to investigate the degree of water absorption of the NR composites filled with PSCG. In general, water molecules penetrate into the filled composites via three different mechanisms: diffusion through micro-gaps between the polymer chains; capillary transport into the micro-gaps; and flaws at the interfaces between filler and matrix (Sreekala et al., 2002; Maslinda et al., 2017; Almansour et al., 2017). Fig. 11 discloses the degree of water absorption as a function of time of the NR composites filled with PSCG and TESPT-treated PSCG. Obviously, degree of water absorption increases rapidly during the first 2 days and tends to slow down afterwards before reaching an equilibrium after 7 days of immersion. At equilibrium state, the unfilled NR composite has the lowest degree of water absorption due to its hydrophobic nature. The degree of water absorption increases continuously with increasing filler loading, regardless of the filler type, which is the consequence from the dilution of the hydrophobic natural rubber by the hydrophilic filler. As the surface treatment of PSCG by TESPT makes the filler become more hydrophobic, TESPT-treated PSCG gives the composites with a slightly lower degree of water absorption, compared to PSCG at the same filler loading.

#### 4. Conclusions

In the present work, purification of SCG by alkalization and bleaching treatment was performed to remove lignin and other nonpolysaccharide components. The percent yield of the purification was 29.5 %. The purified SCG (PSCG) has greater surface roughness leading to higher specific surface area. Results reveal that PSCG contains approximately 30% of cellulose and, thus, 70% of hemicellulose with a trace of nitrogen-containing compounds. Due to the abundance of polar hydroxyl groups, PSCG is incompatible with non-polar rubbers including NR. The poor rubber-filler interaction in conjunction with the low specific surface area of PSCG are the main reasons for poor reinforcement of PSCG. The addition of PSCG into NR results in continuous increases in hardness and modulus together with a progressive decrease in elongation at break. Tensile strength increases with increasing PSCG loading up to 10 phr before declining. Similar trend is also found when PSCG has been treated by TESPT. However, at any given filler loading, TESPT-treated PSCG exhibits greater reinforcement than PSCG as evidenced by the improved modulus, hardness, and tensile strength. Such improvement was thought to arise from the enhanced rubber-filler interaction and the increased crosslink density in the presence of TESPT. Since the TESPT treatment lowers hydrophilicity of PSCG, the NR composites filled with TESPTtreated PSCG possess lower degree of water absorption than those filled with PSCG. Despite the noticeable improvement of reinforcement after the TESPT treatment, PSCG is still considered as an ecofriendly, non-reinforcing filler due to its large particle size and can be used in applications where high mechanical strength is not essential such as floor mats, cow mats, rubber level crossing panels, etc.

#### **Declaration of Competing Interest**

The authors declare that they have no known competing financial interests or personal relationships that could have appeared to influence the work reported in this paper.

#### Acknowledgement

The Materials Chemistry Research Center (MCRC-KKU) and Center of Excellence for Innovation in Chemistry (PERCH-CIC), Department of Chemistry, Faculty of Science, Khon Kaen University are acknowledged for financial and instrument support.

#### References

- Ahmed, K., Nizami, S.S., Raza, N.Z., Shirin, K., 2012. Cure characteristics, mechanical and swelling properties of marble sludge filled EPDM modified chloroprene rubber blends. Adv. Mater. Physics Chem. 2, 90–97. https://doi.org/10.4236/ampc.2012.22016.
- Ahmed, K., Nizami, S.S., Raza, N.Z., Habib, F., 2013. The effect of silica on the properties of marble sludge filled hybrid natural rubber composites. J. King Saud Univ. Sci. 25, 331–339. https://doi.org/ 10.1016/j.jksus.2013.02.004.
- Almansour, F.A., Dhakal, H.N., Zhang, Z.Y., 2017. Effect of water absorption on Mode I interlaminar fracture toughness of flax/basalt reinforced vinyl ester hybrid composites. Compos. Struct. 168, 813–825. https://doi.org/10.1016/j.compstruct.2017.02.081.
- Aguiar, E.C., Gasco, G., Ferreiro, J.P., Mendez, A., 2017. The effect of biochar and compost from urban organic waste on plant biomass and properties of an artificially copper polluted soil. Int. Biodeterior 124, 223–232. https://doi.org/10.1016/j. ibiod.2017.05.014.
- Arifuzzaman Khan, G.M., Alam Shams, M.S., Kabir, M.R., Gafur, M.A., Terano, M., Alam, M.S., 2013. Influence of chemical treatment on the properties of banana stem fiber and banana stem fiber/coir hybrid fiber reinforced maleic anhydride grafted polypropylene/low-density polyethylene composites. J. Appl. Polym. Sci. 128, 1020–1029. https://doi.org/10.1002/app.38197.
- Azwar, E., Hakkarainen, M., 2012. Tuning the mechanical properties of Tapioca starch by plasticizers, inorganic fillers and agrowastebased fillers. ISRN Polym. Sci. 2012,. https://doi.org/10.5402/2012/ 463298 463298.
- Baek, B.S., Park, J.W., Lee, B.H., Kim, H.J., 2013. Development and application of green composites: using coffee ground and bamboo flour. J. Polym. Environ. 21, 702–709. https://doi.org/10.1007/ s10924-013-0581-3.
- Ballesteros, L.F., Teixeira, J.A., Mussatto, S.I., 2014. Chemical, functional, and structural properties of spent coffee grounds and coffee silverskin. Food Bioprocess Technol. 7, 3493–3503. https://doi.org/10.1007/s11947-014-1349-z.
- Ballesteros, L.F., Cerqueira, M.A., Teixeira, J.A., Mussatto, S.I., 2015. Characterization of polysaccharides extracted from spent coffee grounds by alkali pretreatment. Carbohydr. Polym. 127, 347–354. https://doi.org/10.1016/j.carbpol.2015.03.047.
- Banu, J., Kavitha, S., Kannah, R.Y., Kumar, D., Preethi, M., Atabani, A., Kumar, G., 2020. Recycling of spent coffee grounds for useful extracts and green composites. Bioresour. Technol. 302,. https://doi.org/10.1039/d0ra09379c 122821.
- Barana, D., Orlandi, M., Salanti, A., Castellani, L., Hanel, T., Zoia, L., 2019. Simultaneous synthesis of cellulose nanocrystals and a lignin-silica biofiller from rice husk: Application for elastomeric compounds. Ind. Crops Prod. 141,. https://doi.org/10.1016/j.ind-crop.2019.111822 111822.
- Bodirlau, R., Teaca, C.A., Spiridon, I., 2013. Influence of natural fillers on the properties of starch-based biocomposite films. Compos. B. Eng. 44, 575–583. https://doi.org/10.1016/j.compositesb.2012.02.039.
- Boopasiri, S., Sae-Oui, P., Lundee, S., Takaewnoi, S., Siriwong, C., 2021. Reinforcing efficiency of pyrolyzed spent coffee ground in

styrene-butadiene rubber. Macromol. Res. 597–604. https://doi. org/10.1007/s13233-021-9072-x.

- Brendel, O., Iannetta, P.P.M., Stewart, D., 2000. A rapid and simple method to isolate pure alpha-cellulose. Phytochem. Anal. 11, 7–10. https://doi.org/10.1002/(SICI)1099-1565(200001/02)11:13.0.CO;2-
- Conde, T., Mussatto, S.I., 2016. Isolation of polyphenols from spent coffee grounds and silverskin by mild hydrothermal pretreatment. Prep. Biochem. Biotechnol. 46, 406–409. https://doi.org/10.1080/ 10826068.2015.1084514.
- Brown, R.P., Soulagnet, G., 2001. Microhardness profiles on aged rubber compounds. Polym. Test. 20, 295–303. https://doi.org/ 10.1016/s0142-9418(00)00035-0.
- Butler, J., Freakley, P.K., 1992. Effect of humidity and water content on the cure behavior of a natural-rubber accelerated sulfur compound. Rubber Chem. Technol. 65, 374–384. DOI:10.5254/ 1.3538618.
- Cameron, A., O'Malley, S., 2016. Coffee ground recovery program summary report. PLANET ARK 1-18.
- Campos-Vega, R., Loarca-Piña, G., Vergara-Castañeda, H.A., Oomah, B.D., 2015. Spent coffee grounds: A review on current research and future prospects. Trends Food Sci. Technol. 45, 24– 36. https://doi.org/10.1016/j.tifs.2015.04.012.
- Cao, L., Huang, J., Chen, Y., 2018. Dual cross-linked epoxidized natural rubber reinforced by tunicate cellulose nanocrystals with improved strength and extensibility. ACS Sustain. Chem. Eng. 6, 14802–14811. https://doi.org/10.1021/acssuschemeng.8b03331.
- Colantoni, A., Paris, E., Bianchini, L., Ferri, S., Marcantonio, V., Carnevale, M., Palma, A., Civitarese, V., Gallucci, F., 2021. Spent coffee ground characterization, pelletization test and emissions assessment in the combustion process. Sci. Rep. 11, 5119. https:// doi.org/10.1038/s41598-021-84772-y.
- Crumbley, L., 2009. Climate for Action: New Uses for Used Coffee Grounds. Available at: http://blog.epa.gov/blog/2009/02/climatefor-action/ (accessed 2021.12.15.).
- Dannenberg, E.M., 1985. Filler choices in the rubber industry. Rubber Chem. Technol. 55, 860–880. https://doi.org/10.5254/1.3535905.
- Das, O., Bhattacharyya, D., Hui, D., Lau, K.T., 2016. Mechanical and flammability characterizations of biochar/polypropylene biocomposites. Compos. B. Eng. 106, 120–128. https://doi.org/10.1016/ j.compositesb.2016.09.020.
- El Miri, N., Abdelouahdi, K., Zahouily, M., Fihri, A., Barakat, A., Solhy, A., El Achaby, M., 2015. Bio-nanocomposite films based on cellulose nanocrystals filled polyvinyl alcohol/chitosan polymer blend. J. Appl. Polym. Sci. 132, 1–13. https://doi.org/10.1002/app.42004.
- Essabir, H., Hilali, E., Elgharad, A., El Minor, H., Imad, A., Elamraoui, A., Gaoudi, A., 2013a. Mechanical and thermal properties of bio-composite based on polypropylene reinforced with Nut-shells of Argan particles. Mater. Des. 49, 442–448. https://doi.org/10.1016/j.matdes.2013.01.025.
- Essabir, H., Nekhlaoui, S., Malha, M., Bensalah, M.O., Arrakhiz, F. Z., Qaiss, A., Bouhfid, R., 2013b. Bio-composites based on polypropylene reinforced with Almond Shells particles: Mechanical and thermal properties. Mater. Des. 51, 225–230. https://doi.org/10.1016/j.matdes.2013.04.031.
- Essabir, H., Bensalah, M.O., Rodrigue, D., Bouhfid, R., Qaiss, A., 2016. Biocomposites based on Argan nut shell and a polymer matrix: effect of filler content and coupling agent. Carbohydr. Polym. 143, 70–83. https://doi.org/10.1016/j.carbpol.2016.02.002.
- Essabir, H., Bensalah, M.O., Rodrigue, D., Bouhfid, R., Qaiss, A., 2017. A comparison between bio- and mineral calcium carbonate on the properties of polypropylene composites. Construct. Build. Mater. 134, 549–555. https://doi.org/10.1016/j.conbuildmat.2016.12.199.
- Essabir, H., Raji, M., Laaziz, S.A., Rodrique, D., Bouhfid, R., El kacem Qaiss, A., 2018. Thermo-mechanical performances of polypropylene biocomposites based on untreated, treated and

- compatibilized spent coffee grounds. Compos B Eng. 149, 1–11. DOI: 10.1016/j.compositesb.2018.05.020.
- Fernandes, A.S., Mello, F.V.C., Thode Filho, S., Carpes, R.M., Honorio, J.G., Marques, M.R.C., Felzenszwalb, I., Ferraz, E.R.A., 2017. Impacts of discarded coffee waste on human and environmental health. Ecotoxicol. Environ. Saf. 141, 30–36. https://doi. org/10.1016/j.ecoenv.2017.03.011.
- Frost, B.A., Foster, E.J., 2020. Isolation of Thermally Stable Cellulose Nanocrystals from Spent Coffee Grounds via Phosphoric Acid Hydrolysis. J. Renew. Mater. 8 (2), 187–203. https://doi.org/10.32604/jrm.2020.07940.
- Gaidukova, G., Platnieks, O., Aunins, A., Barkane, A., Ingrao, C., Gaidukovs, S., 2021. Spent coffee waste as a renewable source for the production of sustainable poly(butylene succinate) biocomposites from a circular economy perspective. RSC Adv. 11, 18580– 18589. https://doi.org/10.1039/d1ra03203h.
- García-García, D., Carbonell, A., Samper, M.D., García-Sanoguera, D., Balart, R., 2015. Green composites based on polypropylene matrix and hydrophobized spend coffee ground (SCG) powder. Compos. B. Eng. 78, 256–265. https://doi.org/10.1016/j.compositesb.2015.03.080.
- Gardiner, K., Tongeren, M.V., Harrington, M., 2001. Respiratory health effects from exposure to carbon black: results of the phase 2 and 3 cross sectional studies in the European carbon black manufacturing industry. Occup. Environ. Med. 58, 496–503. https://doi.org/10.1136/oem.58.8.496.
- Ghani, H., Abd Karim, S.F., Ramli, R., Musa, M., Jaapar, J., 2019. Effect of bio fillers on mechanical properties of natural rubber latex films. Key Eng. Mater. 797, 249–254. https://doi.org/10.4028/ www.scientific.net/KEM.797.249.
- Hashim, A.S., Azahari, B., Ikeda, Y., Kohjiya, S., 1998. The effect of bis(3-triethoxysilylpropyl) tetrasulfide on silica reinforcement of styrene-butadiene rubber, Rubber Chem. Technol. 71, 289–299. https://doi.org/10.5254/1.3538485.
- Isikgor, F.H., Becer, C.R., 2015. Lignocellulosic biomass: A sustainable platform for production of bio-based chemicals and polymers. Polym. Chem. 6, 4497–4559. https://doi.org/10.1039/ C5PY002631
- Jacques, J. E. "Principles of Compounding" in "Rubber Technology and Manufacturer", C.M. Blow, editor, Butterworths, 1971.
- Kargarzadeh, H., Ahmad, I., Abdullah, I., Dufresne, A., Zainudin, S. Y., Sheltami, R.M., 2012. Effects of hydrolysis conditions on the morphology, crystallinity, and thermal stability of cellulose nanocrystals extracted from kenaf bast fibers. Cellulose 19, 855–866. https://doi.org/10.1007/s10570-012-9684-6.
- Kyung Lee, H., Gi Park, Y., Jeong, T., Seok Song, Y., 2015. Green nanocomposites filled with spent coffee grounds. J. Appl. Polym. Sci. 132, 42043. https://doi.org/10.1002/app.42043.
- Lu, T., Jiang, M., Jiang, Z., Hui, D., Wang, Z., Zhou, Z., 2013. Effect of surface modification of Bamboo cellulose fibers on mechanical properties of cellulose/epoxy composites. Compos. B. Eng. 51, 28– 34. https://doi.org/10.1016/j.compositesb.2013.02.031.
- Lu, T., Liu, S., Jiang, M., Xu, X., Wang, Y., Wang, Z., Gou, J., Hui, D., Zhou, Z., 2014. Effects of modifications of bamboo cellulose fibers on the improved mechanical properties of cellulose reinforced poly(lactic acid) composites. Compos. B. Eng. 62, 191–197. https://doi.org/10.1016/j.compositesb.2014.02.030.
- Machado, E.M.S., Rodriguez-Jasso, R.M., Teixeira, J.A., Mussatto, S. I., 2012. Growth of fungal strains on coffee industry residues with removal of polyphenolic compounds. Biochem. Eng. 60, 87–90. https://doi.org/10.1016/j.bej.2011.10.007.
- Mansor, M.K., Ali, R.C., 2016. Properties evaluation of microcrystalline cellulose and starch as bio-filler in rubber compounding. Adv. Mater. Res. 1133, 593–597. https://doi.org/10.4028/www.scientific.net/amr.1133.593.
- Maslinda, A.B., Abdul Majid, M.S., Ridzuan, M.J.M., Afendi, M., Gibson, A.G., 2017. Effect of water absorption on the mechanical properties of hybrid interwoven cellulosic-cellulosic fibre reinforced

- epoxy composites. Compos. Struct. 167, 227–237. https://doi.org/10.1016/j.compstruct.2017.02.023.
- Massaro Sousa, L., Ferreira, M.C., 2019. Spent coffee grounds as a renewable source of energy: an analysis of bulk powder flowability. Particuology 43, 92–100. https://doi.org/10.1016/j.partic.2018.06.002.
- McNutt, J., He, Q., 2019. Spent coffee grounds: A review on current utilization. J. Ind. Eng. Chem. 71, 78–88. https://doi.org/10.1016/j.jiec.2018.11.054.
- Mokhothu, T.H., John, M.J., 2017. Bio-based fillers for environmentally friendly composites. Handb. Compos. Renewable Mater. 1, 243–270. https://doi.org/10.1002/9781119441632.ch10.
- Mostoni, S., Milana, P., Credico, B.D., Arienzo, M.D., Scotti, R., 2019. Zinc-based curing activators: new trends for reducing zinc content in rubber vulcanization process. Catalysts. 9, 664. https:// doi.org/10.3390/catal9080664.
- Moustafa, H., Guizani, C., Dufresne, A., 2017. Sustainable biodegradable coffee grounds filler and its effect on the hydrophobicity, mechanical and thermal properties of biodegradable PBAT composites. J. Appl. Polym. Sci. 134, 44498. https://doi.org/10.1002/app.44498.
- Murthy, P.S., Naidu, M.M., 2012. Sustainable management of coffee industry by-products and value addition-A review. Resour. Conserv. Recycl. 66, 45. https://doi.org/10.1016/j. resconrec.2012.06.005.
- Mussatto, S.I., Machado, E.M.S., Martins, S., Teixeira, J.A., 2011a. Production, composition, and application of coffee and its industrial residues. Food Bioprocess Technol. 4, 661–672. https://doi.org/10.1007/s11947-011-0565-z.
- Mussatto, S.I., Ballesteros, L.F., Martins, S., Teixeira, J.A., 2011b. Extraction of antioxidant phenolic compounds from spent coffee grounds. Sep. Purif. Technol. 83, 173–179. https://doi.org/10.1016/ j.seppur.2011.09.036.
- Mussatto, S.I., Carneiro, L.M., Silva, J.P.A., Roberto, I.C., Teixeira, J.A., 2011c. A study on chemical constituents and sugars extraction from spent coffee grounds. Carbohydr. Polym. 83, 368–374. https://doi.org/10.1016/j.carbpol.2010.07.063.
- Mussatto, S.I., Machado, E.M.S., Carneiro, L.M., Teixeira, J.A., 2012. Sugars metabolism and ethanol production by different yeast strains from coffee industry wastes hydrolysates. Appl. Energy 92, 763–768. https://doi.org/10.1016/j.apenergy.2011.08.020.
- Niranjan, R., Thakur, A.K., 2017. The toxicological mechanisms of environmental soot (black carbon) and carbon black: focus on oxidative stress and inflammatory pathways. Front. Immunol. 8, 763. https://doi.org/10.3389/fimmu.2017.00763.
- Pujol, D., Liu, C., Gominho, J., Olivella, M.A., Fiol, N., Villaescusa, I., Pereira, H., 2013. The chemical composition of exhausted coffee waste. Ind. Crops. Prod. 50, 423–429. https://doi.org/10.1016/j.indcrop.2013.07.056.
- Ruangudomsakul, W., Ruksakulpiwat, C., Yupaporn, R., 2013. The study of using bio-filler from cassava pulp in natural rubber composites. Adv. Mater. Res. 747, 371–374. https://doi.org/ 10.4028/www.scientific.net/amr.747.371.
- Saba, N., Jawaid, M., Othman, A.Y., Paridah, M.T., 2016. A review on dynamic mechanical properties of natural fibre reinforced polymer composites. Const. Build. Mater. 106, 149–159. https:// doi.org/10.1016/j.conbuildmat.2015.12.075.
- Sae-Oui, P., Sirisinha, C., Hatthapanit, K., Thepsuwan, U., 2005. Comparison of reinforcing efficiency between Si-69 and Si-264 in

- an efficient vulcanization system. Polym. Test. 24, 439–446. https://doi.org/10.1016/j.polymertesting.2005.01.008.
- Santos, R.D., Agostini, D., Cabrera, F., Aparecido, E., Reis, P., Ruiz, M., Budemberg, E., Teixeira, S., Job, A., 2014. Sugarcane bagasse ash: New filler to natural rubber composite. Polimeros. 24, 646–653. https://doi.org/10.1590/0104-1428.1547.
- Segal, L., Creely, J.J., Martin, A.E., Conrad, C.M., 1959. An empirical method for estimating the degree of crystallinity of native cellulose using the X-ray diffractometer. Textile Research Journal 29, 786– 794. https://doi.org/10.1177/004051755902901003.
- Silva, M.A., Nebra, S.A., Silva, M.J.M., Sanchez, C.G., 1998. The use of biomass residues in the brazilian soluble coffee industry. Biomass Bioenergy 14, 457–467. https://doi.org/10.1016/s0961-9534(97)10034-4.
- Sinclair, A., Zhou, X., Tangpong, S., Bajwa, D.S., Quadir, M., Jiang, L., 2019. High-performance styrene-butadiene rubber nanocomposites reinforced by surface-modified cellulose nanofibers. ACS Omega 4, 13189–13199. https://doi.org/10.1021/acsomega.9b01313.
- Siriwong, C., Boopasiri, S., Jantarapibun, V., Kongsook, B., Pattanawanidchai, S., Sae-Oui, P., 2017. Properties of natural rubber filled with untreated and treated spent coffee grounds. J. Appl. Polym. Sci. 135, 46060. https://doi.org/10.1002/app.46060.
- Siriwong, C., Sae-oui, P., Sirisinha, C., 2014. Comparison of coupling effectiveness among amino-, chloro-, and mercapto silanes in chloroprene rubber. Polym. Test. 38, 64–72. https://doi.org/ 10.1016/j.polymertesting.2014.07.003.
- Sreekala, M.S., Kumaran, M.G., Thomas, S., 2002. Water sorption in oil palm fiber reinforced phenol formaldehyde composites. Compos. Part A Appl. Sci. Manuf. 33, 763–777. https://doi.org/10.1016/ s1359-835x(02)00032-5.
- Sung, S.H., Chang, Y., Han, J., 2017. Development of polylactic acid nanocomposite films reinforced with cellulose nanocrystals derived from coffee silverskin. Carbohydr. Polym. 169, 495. https://doi.org/ 10.1016/j.carbpol.2017.04.037.
- Tan, M.Y., Kuan, H.T.N., Khan, A.A., 2017. Tensile properties of ground coffee waste reinforced polyethylene composite. Mater. Sci. 880, 73–76. https://doi.org/10.4028/www.scientific.net/msf.880.73.
- Vaisanen, T., Das, O., Tomppo, L., 2017. A review on new bio-based constituents for natural fiber polymer composites. J. Clean. Prod. 149, 582–596. https://doi.org/10.1016/j.jclepro.2017.02.132.
- Wagner, M.P., 1981. Elastomerics 113, 40. https://doi.org/10.1016/ 0014-3057(94)00156-1.
- Wu, C.S., 2015. Renewable resource-based green composites of surface-treated spent coffee grounds and polylactide: Characterisation and biodegradability. Polym. Degrad. Stab 121, 51–59. https://doi.org/10.1016/j.polymerdegradatab.2015.08.011.
- Xiao, Y., Zou, H., Zhang, L., Ye, X., Han, D., 2020. Surface modification of silica nanoparticles by a polyoxyethylene sorbitan and silane coupling agent to prepare high performance rubber composites. Polymer test. 106195. https://doi.org/10.1016/j. polymertesting.2019.106195.
- Yang, H., Yan, R., Chen, H., Lee, D.H., Zheng, C., 2007. Characteristics of hemicellulose, cellulose and lignin pyrolysis. Fuel 86, 1781–1788. https://doi.org/10.1016/J.FUEL.2006.12.013.
- Zhou, F., Cheng, G., Jiang, B., 2014. Effect of silane treatment on microstructure of sisal fibers. Appl. Surf. Sci. 292, 806–812. https://doi.org/10.1016/j.apsusc.2013.12.054.